Article

The Effect of Amino−Phosphate Interactions on the Biosensing Performance of Enzymatic Graphene Field-Effect Transistors

Gonzalo E. Fenoy,* Esteban Piccinini, Wolfgang Knoll, Waldemar A. Marmisollé, and Omar Azzaroni*

Read Online

ACCESS | 📊 Metrics & More | 📖 Article Recommendations | 🆂🅸 Supporting Information
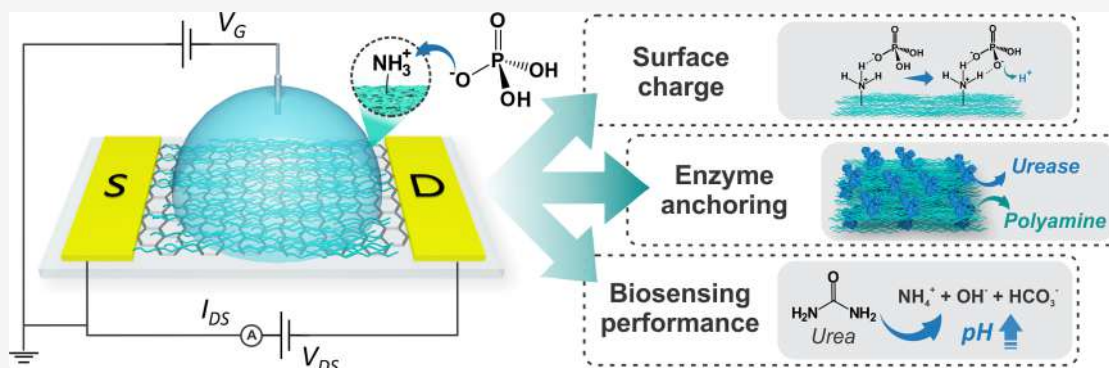
ABSTRACT: The interaction between polyamines and phosphate species is found in a wide range of biological and abiotic systems, yielding crucial consequences that range from the formation of supramolecular colloids to structure determination. In this work, the occurrence of phosphate−amino interactions is evidenced from changes in the electronic response of graphene field effect transistors (gFETs). First, the surface of the transistors is modified with poly(allylamine), and the effect of phosphate binding on the transfer characteristics is interpreted in terms of its impact on the surface charge density. The electronic response of the polyamine-functionalized gFETs is shown to be sensitive to the presence of different phosphate anions, such as orthophosphate, adenosine triphosphate, and tripolyphosphate, and a simple binding model is developed to explain the dependence of the shift of the Dirac point potential on the phosphate species concentration. Afterward, the impact of phosphate−amino interactions on the immobilization of enzymes to polyamine-modified graphene surfaces is investigated, and a decrease in the amount of anchored enzyme as the phosphate concentration increases is found. Finally, multilayer polyamine-urease biosensors are fabricated while increasing the phosphate concentration in the enzyme solution, and the sensing properties of the gFETs toward urea are evaluated. It is found that the presence of simple phosphate anions alters the nanoarchitecture of the polyelectrolyte−urease assemblies, with direct implications on urea sensing.

The interaction between polyamines and phosphates is a decisive type of noncovalent association that shows relevant implications in a wide range of biological systems.[1,2] For instance, nuclear aggregates of biogenic polyamines such as putrescine, spermidine, and spermine and orthophosphate anions (Pi) are present in many replicating cells,[3] and they hierarchically assemble into cyclic structures with high order that are able to protect DNA.[4,5] Moreover, diatom biosilica is mainly constituted of polyamines of up to 20 repeated units and silaffins, and their interaction with phosphate anions (that serve as ionic cross-linkers) yields aggregates that determines the species-specific patterning of diatom biosilica.[6,7] In addition, polyamine−phosphate interactions have also been used to fabricate abiotic functional structures, such as tunable supramolecular films,[1,8] which can modulate cell adhesion and proliferation.[9] Furthermore, polyamine−phosphate-based systems have also been employed for the construction of drug delivery systems, showing an excellent ability to encapsulate

chemotherapeutic agents such as curcumin and doxorubicin.[10] Similarly, poly(allylamine)−Pi (PAH-Pi) nanoparticles have been employed as carriers for silencing RNAs,[11] for the straightforward preparation of underwater adhesives,[12] as well as sorbents for dyes.[13]

The relevance of these interactions roots on the particular features that they present since phosphates generate assemblies with polyamines more effectively than other polyvalent anions.[14] In this regard, it has been proposed that the interaction with protonated amines promotes the dissociation
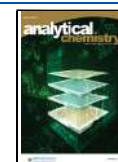
of phosphate species.[14] Moreover, while electrostatic interactions are perhaps the major driving force for the generation of polyamine–phosphate assemblies, hydrogen bonds are also believed to be essential to stabilize their structure.[1] Hence, when the Pi–amino interaction was studied on surfaces, a complex dependence of the surface effective charge on pH was obtained.[15]

Another interesting outcome of these interactions, especially when considering assemblies on surfaces, involves the charge reversion phenomenon, i.e., as a result of phosphate binding, previously positively charged polyamine-modified surfaces develop a negative excess charge in the presence of phosphates in solution,[16–18] which has important repercussions regarding their further interaction with biomolecules.[18,19] It has been reported that the charge reversion effect occurs in the physiological phosphate concentration range, enhancing its biological importance.[14] For instance, the Pi-driven surface charge reversion of amino-terminated self-assembled monolayers allows their further interaction with positively charged proteins such as cytochrome c (cyt-c).[19,20] Polyamine–phosphate interactions have also been shown to provoke charge reversion in layer-by-layer assemblies,[16] as well as in polyamine-modified silica NPs.[14] Similarly, these interactions significantly modified the rectification properties of solid-state nanochannels (SSNs).[18]

On the other hand, graphene field-effect transistors (gFETs) have gained much attention in the last decade since they provide highly sensitive and fast detection of analytes in real-time, and they can also be easily miniaturized.[21,22] As a result, gFETs are one of the most promising technologies for the development of point-of-care devices and mobile health technologies.[23,24] Briefly, gFET-based sensors make use of the variation in the resistance of the graphene channel that happens upon the adsorption/recognition of the analyte, and this change is immediately amplified by the field-effect, yielding very sensitive devices.[22,25,26] Hence, gFETs have been employed to sense a wide range of analytes, such as ions, molecules, and relevant biomarkers.[23,25,27] Among them, acetylcholine, glucose, and urea have been successfully detected by enzymatic gFETs.[22,28,29]

When considering the performance of the enzymatic gFET biosensors, a proper enzyme anchoring is key to fabricate reliable and sensitive devices since most of their analytical figures of merit critically depend on enzyme stability.[22,30,31] The immobilization approach should not disrupt the activity of the enzyme and the accessibility to its active sites while conserving the functionality of the transducing element.[32] In this respect, covalent anchoring can present some obstacles, such as poor reproducibility and the threat of affecting the structure (and therefore the activity) of the enzyme, since crucial moieties could be involved in the immobilization procedure.[33–35] In addition, the covalent anchoring of enzymes to graphene has been reported to affect the sp² structure of the channel material, negatively affecting the signal transduction mechanism of the biosensors.[36]

In contrast, enzyme immobilization through electrostatic interactions does not usually disturb its native structure nor the semiconducting properties of the transistor.[22,37] In this regard, the modification of surfaces with polyamines has been reported as an interesting approach to electrostatically immobilize different enzymes, such as arginase, urease, glucose oxidase (GOx), and acetylcholinesterase.[22,28,30,38] Similarly, the multilayer assembly of urease and polyamines has been shown to

ensure proper enzymatic activity and accessibility of the substrate to the active sites.[28] In addition, the use of polyamines amplifies the pH sensitivity of gFETs by (de)protonation of the charged moieties, thus resulting in an additional electrostatic gating.[39]

In this regard, it is well-known that the occurrence of phosphate interactions with amino moieties can disturb the anchoring of bioentities such as DNA, enzymes, and other functional proteins.[14,19,40] Particularly, it has been stated that Pi–amino interactions hinder GOx electrostatic adsorption on polyamine-modified Au surfaces.[14] Hence, the study of these interactions in gFETs is of major relevance, having key potential consequences in the biosensing field. Finally, the fabrication of a gFET–ferritin platform for the detection of phosphate anions in water has been reported,[41] and the detection of different nucleoside triphosphates by gFETs has been recently described.[42] To the best of our knowledge, the occurrence of polyamine-phosphate interactions in gFETs has not been studied so far.

In this work, different aspects of phosphate–amino interactions on gFETs are studied. First, gFETs are modified with sodium 1-pyrenesulfonate (SPS), and a layer of poly(allylamine) (PAH) is deposited to confer amino moieties to the surface. Next, the effect of different phosphate anions such as orthophosphate, tripolyphosphate (TPP), and adenosine triphosphate (ATP) on the transfer characteristics of the devices is studied. Moreover, a simple model is developed to account for the variations in the Dirac point potential (V_i) of the transistors upon phosphate binding. Later, the influence of Pi–amino interactions on the enzyme anchoring to PAH-graphene surfaces is studied by surface plasmon resonance (SPR). Finally, urea biosensors are fabricated through the deposition of urease–polyamine multilayers, and the influence of the phosphate–amino interactions on the urea-sensing performance of the devices is examined.

■ MATERIALS AND METHODS

gFETs and Electrical Measurements. Reduced graphene oxide (rGO) FETs, prepared by a previously reported wafer-scale method, were supplied by GISENS BIOTECH (Argentina).[43] A Ag/AgCl reference electrode (Micrux, Spain) was used as the gate electrode. Electrolyte-gated gFET measurements (I_{DS}–V_G and I_{DS}–time curves) were performed using a Teq4 bipotensiostat (nanoTeq, Argentina). A source-drain potential (V_{DS}) of 100 mV was employed for all the measurements. For the evaluation of the transfer characteristics (I_{DS}–V_G curves) in the presence of Pi, TPP, and ATP, different anion concentration solutions were prepared in 10 mM KCl, adjusted to pH 7 and added to the cell to reach the final concentration. For the urea static sensing experiments, different analyte solutions were prepared in 10 mM KCl, the pH was adjusted to 7, and the solution was added to the cell to reach the final concentration. For the urea chronoamperometric (I_{DS}–time) sensing, the gate potential (V_G) was kept at −200 mV, and different urea solutions were added to the cell to reach the final concentration.

Fabrication of the Urea Biosensors. To fabricate the urea biosensors, bare gFETs were first functionalized with SPS by overnight incubation in a 5 mM SPS solution in DMF and rinsed three times with DMF and then with deionized water. Next, the multilayer (PAH/Urease)$_n$ assemblies were assembled by dip-coating: First, the gFETs were dipped in 1
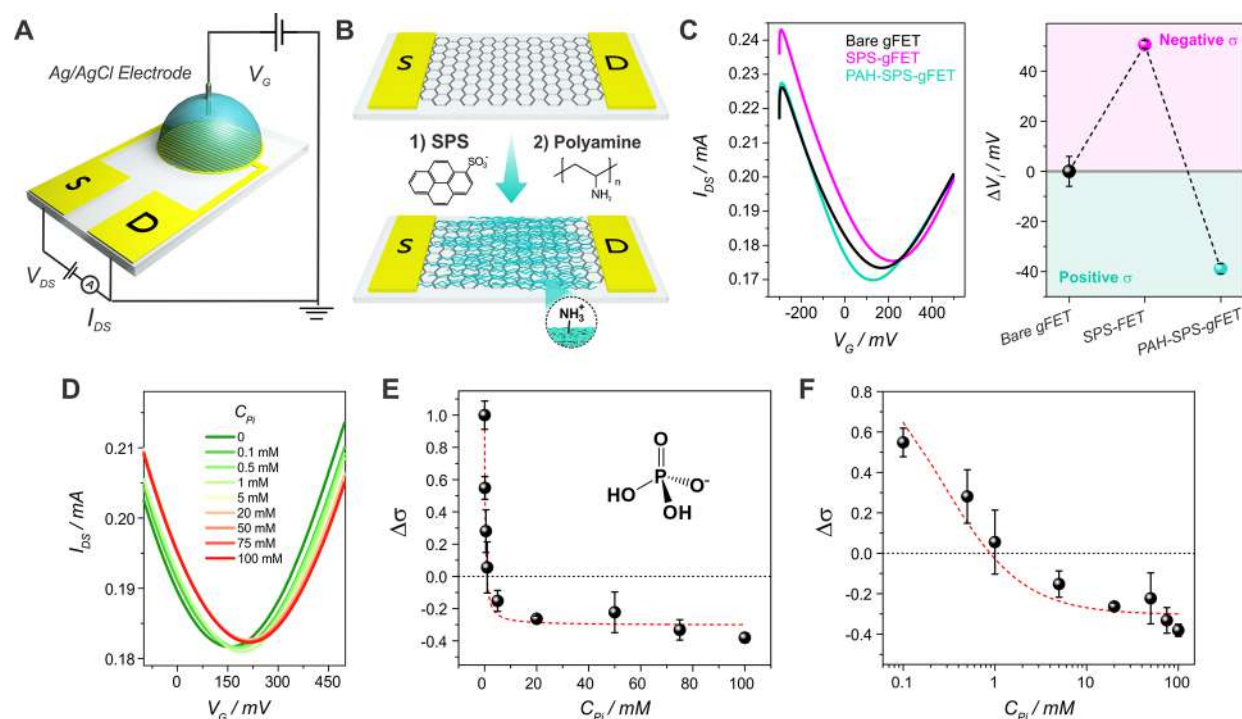
Figure 1. Illustration of the electrolyte-gated configuration employed for the gFET measurements (A). Scheme of the modification process of the gFETs (B). Transfer characteristics (left) and shift of the V_i (right) for a bare gFET and after each modification step (V_{DS} = 100 mV, 10 mM KCl, pH 7) (error for two measurements) (C). Transfer characteristics of a PAH-modified gFET for different Pi concentrations (V_{DS} = 100 mV, 10 mM KCl, pH 7) (D). Relative surface charge variation different Pi concentrations together with the curves obtained for the fitting in a linear (E) and logarithm scale (F) (n = 2).

mg/mL PAH in Milli-Q for 10 min. Next, they were soaked in Milli-Q for 5 min and immersed in urease (1 mg/mL) in 0.1 M KCl (pH 7) solution with 0, 10, and 50 mM Pi. Later, the gFETs were rinsed with 0.1 M KCl pH 7 with 0, 10, and 50 mM Pi, respectively, for 5 min. This process constituted one bilayer, and it was repeated two more times to yield (PAH/Urease)$_3$-gFETs. The biosensors were stored at 4 °C.

SPR Measurements. Commercial SPR Au substrates (SPR102 AU, BioNavis) were first modified with cysteamine and then with rGO, as previously reported.[22,38] The rGO-modified substrates were washed with water and dried with N$_2$. Next, the same procedure employed for the SPS-modification of the gFETs was followed. Later, the SPS–rGO–Au substrates were mounted on the SPR apparatus, and the functionalization with PAH and urease was performed. A 1 mg/mL urease solution in 0.1 M KCl (pH 7.4) was employed, while the Pi concentration in the solution was varied from 0 to 50 mM. The enzyme surface coverage was calculated using:

$$\Gamma_p = \frac{\Delta\theta \times k \times d_p}{dn/dc}$$

where $k \times d_p$ is 1.9×10^{-7} cm/° (at 785 nm) and dn/dc is 0.182 cm^3 g^{-1} for globular proteins. For the estimation of the PAH surface coverage, a dn/dc value of 0.197 cm^3 g^{-1} was employed.[44] Thus, Γ_p obtained for PAH was $1.82 \cdot 10^{-7}$ g/cm^2. Moreover, the rGO and polyamine thicknesses were estimated by fitting the SPR curves with the Winspall software. A n = 2.2 was employed for rGO,[45] while n = 1.465 was used for the PAH layer.[46] Next, a thickness of 1.9 nm was obtained for the PAH layer, in good agreement with previous reports.[47,48] For the (PAH/Urease)$_3$ assembly, a thickness of 48 nm was

obtained from SPR measurements by using n = 1.45 for the enzyme layer.[49]

RESULTS AND DISCUSSION

gFET Characterization and Functionalization. The electrical characterization of the gFETs was performed employing an electrolyte-gated setup (Figure 1A). To confer sulfonate moieties to the graphene surface for the subsequent polymer anchoring, the gFETs were functionalized with SPS (Figure 1B), yielding a negatively charged surface, as shown in Figure 1C. Next, the V_i of the transistors (Figure 1C, right) shifted to more positive values (ca. +50 mV), which is coherent with the n-type doping of the graphene channel caused by the negative charges from the sulfonate moieties in SPS.[50]

The further electrostatic adsorption of a polyamine (PAH) yielded a positively charged surface as evidenced by the transfer characteristics shown in Figure 1C (AFM measurements of the channel of the PAH-SPS-gFETs are shown in Figure S2). Upon PAH adsorption, the V_i shifts negatively by ~40 mV (compared with the V_i of the bare gFETs), which is ascribed to the p-type doping of the gFETs due to the positive charges incorporated by the polyamine. It should be noted that the surface charge caused by the anchoring of the pyrene molecules is totally reverted when the polyelectrolyte is adsorbed, leading to a positively charged surface.[50] Correlations between the surface charge density and V_i shifts explained here will be further used to interpret the changes in the transfer characteristics caused by the occurrence of amine–phosphate interactions.

Effect of Pi Binding on gFETs. Next, the effect of amino–phosphate interactions on gFETs was investigated. The

transfer characteristics of a polyamine-modified gFET at different Pi concentrations (10 mM KCl, pH 7) are shown in Figure 1D. Upon increasing the Pi concentration in the electrolyte solution, the V_i of the PAH-gFETs shifts to more positive values, in agreement with n-type doping of the graphene channel. Then, a diminution of the positive charges of the polyelectrolyte is inferred, ascribed to the interaction of phosphate anions with the amino moieties. These results are in line with those observed in different surface charge-sensitive systems, such as PAH-modified silica NPs,[14] and SSNs.[18] Moreover, it can be seen that the strong phosphate−amine interaction not only electrostatically screens the (positive) surface charge incorporated by the polyamine but also causes its reversion, yielding a negatively charged surface (that is, the V_i of the transistors moves to more positive values than that of the bare gFETs). This charge reversal phenomenon has very relevant functional consequences in a wide variety of systems.[19]

Next, and based on previous works,[14,18] we developed a simple model that accounts for the phosphate−amino interactions in the polyamine-modified gFET surface. Briefly, the model describes the V_i (and therefore, the surface charge) dependence on the occurrence of the amino-phosphate interactions, and it is described in the SI. Subsequently, the experimental results for the V_i shifting were adjusted to the developed model through non-linear fitting according to eq 1:

$$\frac{\Delta V_i}{\Delta V_i^0} = \frac{1 - C[\text{Pi}]}{1 + B[\text{Pi}]} \quad (1)$$

where ΔV_i is the shift of the V_i observed for a given Pi concentration, ΔV_i^0 is the V_i shift in the absence of Pi, [Pi] is equal to the total phosphate concentration, and B and C are constants for a given pH value. From the fitting of the experimental data to eq 1, it is possible to obtain the anion phosphate species concentration necessary to induce a zero-surface charge as $[\text{Pi}]_0 = 1/C$ and the charge reversion degree as $R(\%) = 100(C/B)$.

The relative variation in surface charge ($\Delta V_i/\Delta V_i^0$) obtained from the shifting of V_i upon increasing Pi concentration together with the obtained curves for the fitting of eq 1 are shown in Figure 1E, while Figure 1F shows the results in a logarithm scale. The results for the parameters obtained from the fitting are shown in Table 1. It can be observed that the

Table 1. Parameters Obtained from the Fitting of the Shift of V_i upon Increasing Phosphate Concentration to the Binding Model

anion	B	C	$[\text{An}]_0$	R (%)
Pi	3.7 ± 1.2	$1.1 \pm 0.3 \ \text{mM}^{-1}$	$0.9 \pm 0.3 \ \text{mM}$	29.7
TPP	0.11 ± 0.03	$0.11 \pm 0.03 \ \mu\text{M}^{-1}$	$9 \pm 3 \ \mu\text{M}$	100
ATP	0.15 ± 0.01	$0.11 \pm 0.01 \ \mu\text{M}^{-1}$	$9.1 \pm 0.8 \ \mu\text{M}$	73.3

fitting matches the experimental data, indicating that the developed binding model quantitatively describes the V_i shifting behavior. Moreover, it can be observed that a concentration of Pi of ∼1 mM induces a zero-charge surface on the gFETs at the employed ionic strength. This outcome could have significant consequences as Pi species are present in the widely employed PBS buffer.[51] Next, the use of a 1/10 dilution of the buffer would already neutralize the charge of the PAH-modified surface, altering the interaction of the graphene

channel with the bioentities and, thus, the sensing performance of the devices.

Furthermore, at higher Pi concentration values, the surface charge reverses its values, yielding a surface with a negative charge of approximately 30% of the original positive charge (Figure 1E and Table 1). This effect has also been observed in a variety of PAH-modified surfaces, such as multilayer assemblies, silica particles, and SSNs.[14,16,17] The shift of V_i can be unequivocally ascribed to the Pi binding to the amine-functionalized surfaces as no considerable shifting of the V_i of a SPS-modified gFET was observed upon the addition of different phosphate species to the electrolyte solution (Figure S1).

Other Phosphate Species. Next, we extended the study of the effect of phosphate−amino interactions on gFETs to other phosphate species. In this regard, it is well known that TPP presents strong interactions with polyamines (and particularly with PAH).[12] Therefore, TPP was employed to account for the binding of polyphosphate species displaying multivalent interactions with PAH adsorbed on the gFETs. The measurements were performed at pH 7, where TPP is mostly in the tri- and tetravalent anionic states. From Figure 2A, it can be observed that, as similarly seen for Pi, the V_i of the polymer modified-gFETs shifts to more positive values upon TPP addition, in agreement with a n-type doping of the graphene channel. This result can be ascribed to the interaction of TPP anions with the amino moieties present in the polyamine, causing a diminution of the exposed positive charges. In addition, the TPP binding also causes the reversal of the electrostatic charge, yielding a negatively charged surface. However, significant quantitative differences with respect to the results reported in Figure 2 for Pi can be noticed. The first one involves the lower concentration range in which the interactions are observed since the shift of the V_i occurs upon adding TPP concentrations in the micromolar range. This outcome is expected when considering the higher negative charge of the TPP molecule at pH 7. In this regard, the strong interaction between TPP and different polyamines as PAH and dendrigraft poly-L-lysine has been widely studied,[10,52] and a very similar behavior was observed when studying TPP-PAH interactions in SSNs.[18] Furthermore, from Figure 2B,C and Table 1, it can be observed that the degree of charge reversal reaches 100% for TPP, higher than that observed for Pi (∼30%), which also accounts for the stronger interaction between TPP with PAH.

To gain further insight into the binding of biologically relevant polyphosphates species on amine-functionalized gFETs, we studied the interaction of ATP with the PAH-gFETs. The relevance of ATP is well known, being responsible for the regulation of various biological processes since it is the major energy source of cells, and its concentration has been found to be closely related to many diseases such as hypoglycemia and even some malignant tumors.[42,53] Next, the effect of ATP concentration on the transfer characteristics of PAH-gFETs was studied as performed for Pi and TPP. From Figure 2D, it can be observed that, similarly to what was observed for the other phosphate species, the addition of ATP to the electrolyte solution causes the shift of V_i to more positive values. Moreover, the changes occur for the same concentration values than those observed for TPP, yielding a quantitatively similar anion concentration value for the zero surface charge (Figure 2E,F and Table 1). This result also supports the application of the binding model for biorelevant
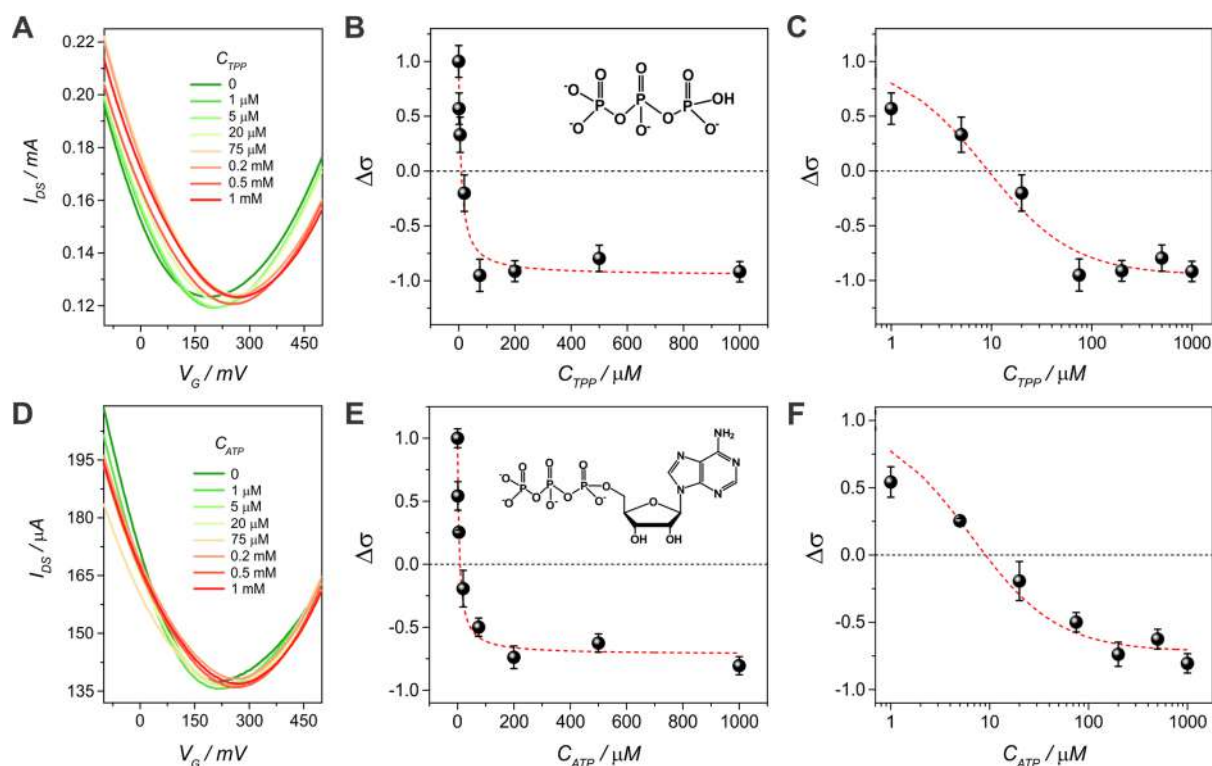
Figure 2. Transfer characteristics of a PAH-modified gFET for different anion concentrations (V_{DS} = 100 mV, 10 mM KCl, pH 7); relative surface charge variations obtained from the shift of the V_i of the devices upon different anion concentrations together with the curves obtained for the fitting in a linear and logarithm scale for TPP (A−C) and ATP (D−F) (n = 2).
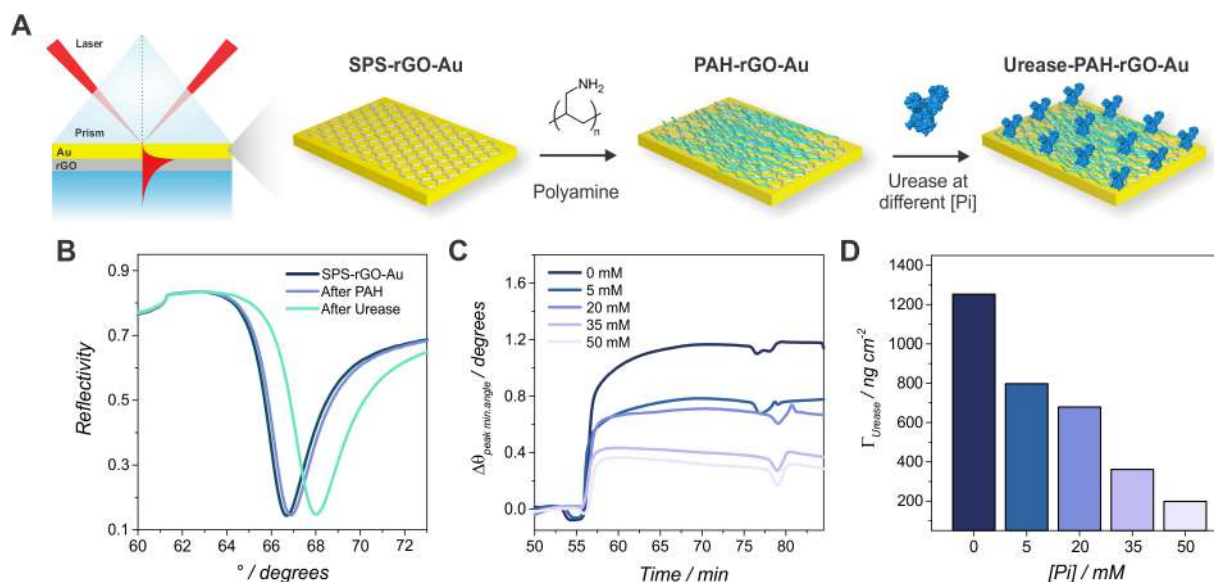
Figure 3. Scheme of the SPR setup employed and the functionalization steps for the Au SPR substrates (A). Example of SPR curves of a rGO-modified SPR substrate for the different functionalization steps (curves for urease anchoring at 5 mM Pi) (B). Change in the minimum reflectivity angle of the SPR scan for the urease anchoring on PAH-modified rGO-Au SPR substrates performed with solutions with different Pi concentrations (C). Urease surface coverage obtained from the SPR measurements (D).

species. On the other hand, the charge reversion degree reaches ~75% for ATP, while the value obtained for TPP is higher (100%). This outcome can be due to the amino moiety present at the adenine residue of ATP, which provokes a lower negative density charge compared with TPP.

Interestingly, these findings could pave the way for the fabrication of sensors of ATP and other biorelevant nucleoside triphosphates, such as guanosine-5′-triphosphate, cytidine-5′-triphosphate, uridine-5′-triphosphate, and thymine-5′-triphosphate.[42] Finally, it is worth noting that results for the binding constants determined here (in 10 mM KCl) are higher than those reported for SiO$_2$ microparticles and SSNs (obtained in 100 mM KCl solutions), as could be expected from the effect of the ionic strength on the ionic association.[14,18]

Influence of Pi on Enzyme Anchoring. Another relevant impact of Pi−amino interactions involves the immobilization
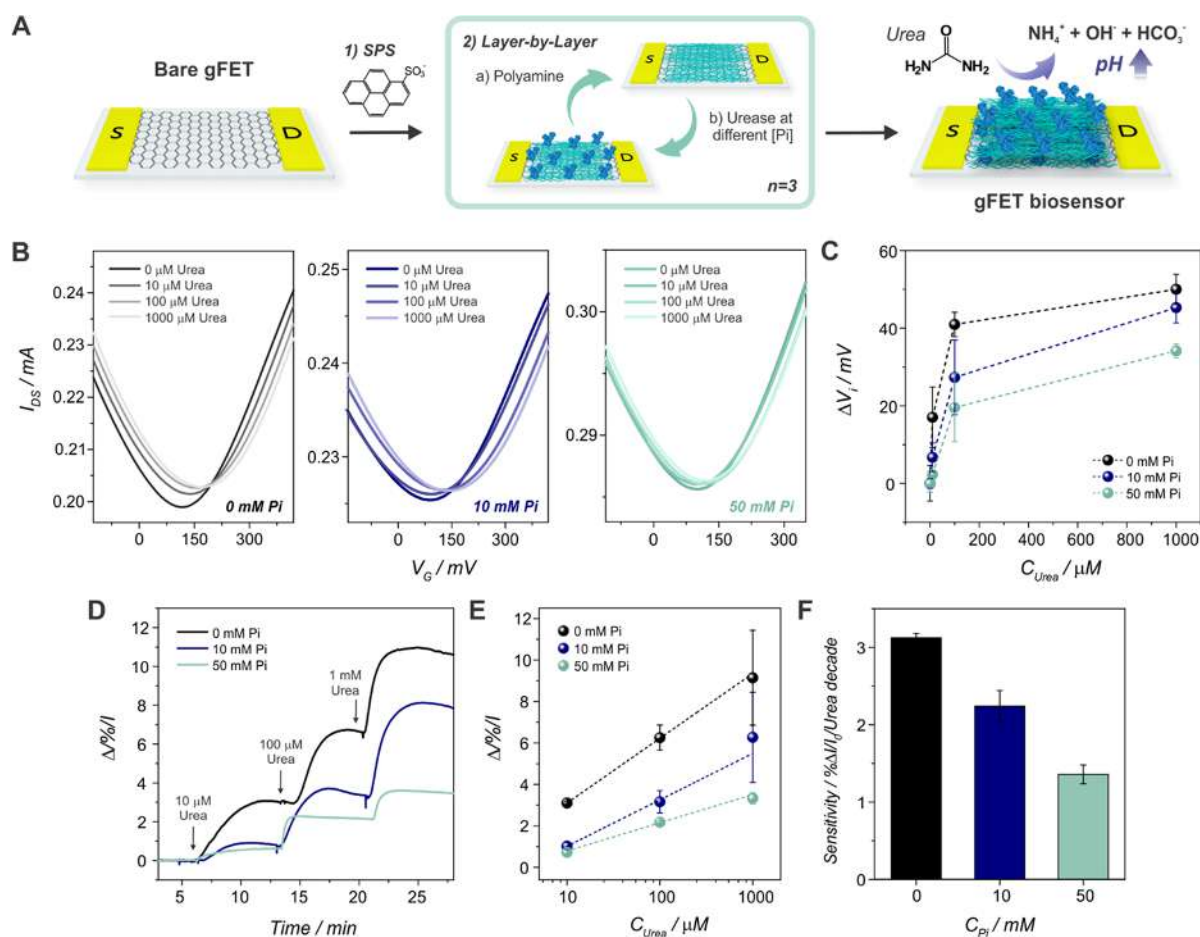
Figure 4. Illustration of the fabrication of the biosensors and the urea catalysis reaction (A). Transfer characteristics for a (PAH/Urease)$_3$-gFET assembled at urease solutions with 0, 10, and 50 mM Pi for different urea concentrations (V_{DS} = 100 mV, 10 mM KCl, pH 7) (B). Shift of the V_i obtained from the transfer characteristics in a linear scale (average from two electrodes, average of three curves each for each Pi concentration) (C). Relative I_{DS} change for three (PAH/Urease)$_3$-gFETs assembled at urease solutions with 0, 10, and 50 mM Pi upon the addition of different urea concentration solutions (V_G = −200 mV, V_{DS} = 100 mV, 10 mM KCl, pH 7) (D). Biosensors' relative drain-source response in a logarithmic scale (E) and sensitivity (F) obtained from the linear fitting of the data in plot 5 (E) (average for two different electrodes for each Pi concentration employed).

of biomolecules on surfaces since they influence the anchoring of bioentities such as DNA and cyt-c.[19,40] In addition, it has been shown that Pi−amino interactions diminish the amount of electrostatically immobilized GOx on polyamine-modified surfaces due to surface charge neutralization (and reversal) upon phosphate exposure.[14]

Next, the influence of Pi concentration on the electrostatic immobilization of urease on PAH-modified graphene surfaces was studied by SPR. To this end, urease solutions with increasing Pi concentration were flown and the amount of anchored enzyme was evaluated. The solution pH was maintained at 7.4 since this is the value of the physiological pH and the pH value of 1xPBS.

Moreover, as the isoelectric point of urease is known to be between 5.0 and 5.2,[54] it will bear negative charges at this pH and, consequently, it will adsorb mainly by electrostatic interactions to the polyamine (Figure 3A). Figure 3B shows examples of the reflectivity curves obtained for each functionalization step of the rGO−Au substrates, while Figure 3C shows the angular scan (change in the minimum reflectivity angle) for the urease anchoring at different Pi concentrations. The obtained surface coverage values for urease in free Pi solution are in good agreement with those recently reported.[39]

Next, from Figure 3D, it can be seen that the amount of immobilized urease diminishes upon increasing the Pi concentration in the buffer (relative changes with respect to 0 mM Pi are shown in Figure S3). This effect can be ascribed to the partial neutralization of the positive charges of the amino-functionalized surface by Pi, thus hindering enzyme anchoring. This effect has been recently reported for the adsorption of GOx on amino-modified Au surfaces.[14]

Moreover, from Figure 3D, it is observed that at the relatively low phosphate concentration of 5 mM, the immobilization of the enzyme already diminishes by ~36%. This result exhibits the relevance of the Pi−amino interactions since the addition of 5 mM Pi produces a significant decrease in protein adsorption, while it just means a minor increment in the ionic strength of the solution. In this regard, PBS is a widely employed buffer in biochemical and biological research, which contains 10 mM Pi +137 mM NaCl + 2.7 mM KCl.[51] Thus, the relevance of the interactions must be considered when immobilizing enzymes or biomolecules on amino-functionalized surfaces while employing this buffer, as a 1:2 dilution would already involve a considerable decrease in the amount of anchored biomolecules.

Furthermore, it is observed that even at high Pi concentrations, some amount of urease is still adsorbed. This result suggests that, while the electrostatic interactions are the main forces intervening in the anchoring of the enzyme, other interactions could also be taking place (since the surface at this pH and Pi concentration should be exposing negative charges[14]). Finally, the results account for the relevance of the phosphate binding on amino-modified surfaces since it drastically changes the surface charge, consequently affecting its further interaction with biomolecules. Since the functionalization with polyamines is a well-known strategy for the anchoring of biological entities in all kinds of surfaces (and particularly, graphene)[1,22,30] and PBS is a widely employed buffer for enzyme immobilization,[55,56] we believe that this outcome will be especially meaningful for fields that deal with the anchoring of enzyme to surfaces, such as biosensing.

Effect of Pi−Amino Binding on Urea Sensing. The immobilization of enzymes through electrostatic interactions on polyamine-modified surfaces is a very effective approach to construct gFET-based biosensors.[22] Particularly, the fabrication of multilayer assemblies of urease and polyamines on gFETs has been used to fabricate urea sensors.[28] Next, to study the effect of Pi concentration on the fabrication of PAH/urease multilayer assemblies on gFETs and its consequences on the biosensing performance of the transistors, the assembly of three (PAH/Urease) bilayers on gFETs ((PAH/Urease)$_3$-gFETs; AFM measurements of the channel are shown in Figure S2) was performed while varying the Pi concentration from 0 to 50 mM in the urease solution, and their urea detection performance was studied (Figure 4A).

Figure 4B shows the urea response in terms of the transfer characteristics of (PAH/Urease)$_3$-gFETs assembled using different Pi concentration in the urease solution. Upon urea adding, the V_i shifts to more positive potentials. This behavior has been ascribed to the increase of the local pH generated upon the enzyme-catalyzed hydrolysis, generating NH_4^+, HCO_3^-, and OH^-.[28,57] Furthermore, from Figure 4C, it is noted that the shift of the V_i for the different urea concentrations diminishes upon increasing the Pi concentration in the urease solution. This is in line with the findings previously shown, indicating that the gFETs assembled with Pi in the urease solution have a lower amount of enzyme and, therefore, show lower response to urea. A quantitative comparison of the response of the biosensors assembled with 10 mM Pi with the ones assembled without Pi yields that the average diminution of the shifting of V_i for all urea concentrations reaches 35% (Figures S6 and S7). Similarly, the devices assembled with 50 mM Pi show an even smaller shift of V_i. When comparing the response of these biosensors with those assembled without Pi, the average diminution of the V_i shifting for all the urea concentrations reaches 75% (a more detailed analysis is found in the SI). It should be noted here that even the sensors fabricated employing 50 mM Pi in the urease solution show a response to urea addition. These findings are consistent with the SPR results, which showed that the adsorption of urease occurs on the polyamine-modified graphene surface even when employing solutions with 50 mM Pi.

Next, the effect of the presence of Pi in the urease assembly solution on the biosensing performance of the gFETs was also studied for measurements performed at a fixed V_G (Figure 4D and Figure S5). The catalysis of the enzyme substrate causes an increase in the local pH, shifting the V_i of the sensors to more positive values. Later, when biasing the transistors at a more negative fixed gate potential than V_i (that is, the hole regime, where $V_G < V_i$) at a $V_{DS} > 0$, an increase of I_{DS} is observed upon urea addition. From Figure 4D,E, similar results to those reported for the shift in the V_i were obtained: the addition of Pi to the urease solution implies a lower amount of assembled enzyme in the multilayer films and, therefore, a lower response to urea. The comparative results for both assembly conditions and every urea concentration are shown in Figure S6. When comparing the response of the biosensors assembled with 10 mM Pi with the ones assembled without Pi, the average diminution of the response for all the urea concentrations reaches 49%. For those sensors fabricated employing 50 mM Pi, the average diminution of the relative change of I_{DS} for all the urea concentrations reaches 69% (Figure S7). Similar results are observed from the linear fitting of the change in I_{DS}, where the biosensors assembled without Pi show the highest sensitivity, while it diminishes upon increasing Pi concentration (Figure 4F).

In addition, it can be noted that for multilayer assemblies prepared in the absence of Pi, the monitoring of I_{DS} shows proper linearity, while the monitoring of the V_i resulted in sublinear behavior (Figure S4). This difference may be explained as follows: due to the hydrolysis of urea, the $I_{DS}-V_G$ curves shift to more positive V_G values, while a slight increase of I_{DS} is also observed (e.g., at the Dirac point, the minimum current value, I_{min}, increases). As described elsewhere,[58] this phenomenon may occur due to a decrease of the charged impurities scattering caused by the increase of pH. Therefore, when the sensing response is monitored in terms of I_{DS}, the two phenomena are displayed in the signal; thus, the sensing behavior may show some differences depending on the chosen monitoring parameter.

In summary, the relevance of the Pi−amino interactions occurring in the assembly process of the multilayer architecture is evidenced since the performance of the biosensors toward urea sensing clearly worsens when increasing the Pi concentration. It is observed that the use of a well-known buffer as PBS for urease immobilization can dramatically affect the response of the biosensors, yielding diminutions that range from 35 to 50% depending on the measurement setup employed.

■ CONCLUSIONS

In summary, we have studied the effect of Pi−amino interactions on polyamine-modified gFETs and developed a simple model that explains their impact on the surface charge. Phosphate species such as orthophosphate, TPP, and ATP strongly interact with the amino moieties, yielding not only the screening of the positive charges but also the charge reversal of the surface. It was also revealed that the electrostatic immobilization of urease to amino-modified surfaces is drastically affected when increasing the Pi concentration in the enzyme solution due to those interactions. It was shown that relatively low concentrations of Pi, as those employed in the common PBS buffer, greatly diminish the amount of anchored urease. Later, multilayer polyamine−urease biosensors were fabricated, and it was shown that their performance worsened as the Pi concentration increased due to the decreased amount of enzyme immobilized on the transistors.

These results illustrate the potential of the combination of rationally designed coatings and gFETs for studying phys-

icochemical phenomena with implications in sensing applications. The influence of phosphate species on the assembly behavior of the macromolecules observed reinforces the word of caution about the use of PBS and other phosphate-containing solutions when studying supramolecular systems in which amino-bearing entities are involved. Future work will be directed toward the effects of these interactions on other biosensing devices such as polyamine-modified organic electrochemical transistors.

ASSOCIATED CONTENT

Supporting Information

The Supporting Information is available free of charge at https://pubs.acs.org/doi/10.1021/acs.analchem.2c02373.

> Amino-phosphate binding model, control experiments, and further analysis of the performance of the biosensors (PDF)

AUTHOR INFORMATION

Corresponding Authors

Gonzalo E. Fenoy − *Instituto de Investigaciones Fisicoquímicas Teóricas y Aplicadas (INIFTA), Universidad Nacional de La Plata (UNLP), CONICET, 1900 La Plata, Argentina; AIT Austrian Institute of Technology GmbH, 3430 Tulln, Austria;* orcid.org/0000-0003-4336-4843; Email: gonzalofenoy@inifta.unlp.edu.ar

Omar Azzaroni − *Instituto de Investigaciones Fisicoquímicas Teóricas y Aplicadas (INIFTA), Universidad Nacional de La Plata (UNLP), CONICET, 1900 La Plata, Argentina; CEST-UNLP Partner Lab for Bioelectronics (INIFTA), La Plata 1900, Argentina;* orcid.org/0000-0002-5098-0612; Email: omarazzaroni@quimica.unlp.edu.ar

Authors

Esteban Piccinini − *Instituto de Investigaciones Fisicoquímicas Teóricas y Aplicadas (INIFTA), Universidad Nacional de La Plata (UNLP), CONICET, 1900 La Plata, Argentina*

Wolfgang Knoll − *AIT Austrian Institute of Technology GmbH, 3430 Tulln, Austria; Department of Scientific Coordination and Management, Danube Private University, 3500 Krems an der Donau, Austria;* orcid.org/0000-0003-1543-4090

Waldemar A. Marmisollé − *Instituto de Investigaciones Fisicoquímicas Teóricas y Aplicadas (INIFTA), Universidad Nacional de La Plata (UNLP), CONICET, 1900 La Plata, Argentina;* orcid.org/0000-0003-0031-5371

Complete contact information is available at:
https://pubs.acs.org/10.1021/acs.analchem.2c02373

Author Contributions

The manuscript was written through the contributions of all authors. All authors have given approval to the final version of the manuscript.

Notes

The authors declare no competing financial interest.
http://softmatter.quimica.unlp.edu.ar; TW: @softmatterlab

REFERENCES

(1) Marmisollé, W. A.; Irigoyen, J.; Gregurec, D.; Moya, S.; Azzaroni, O. *Adv. Funct. Mater.* 2015, 25, 4144−4152.
(2) Di Luccia, A.; Picariello, G.; Iacomino, G.; Formisano, A.; Paduano, L.; D'Agostino, L. *FEBS J.* 2009, 276, 2324−2335.
(3) D'Agostino, L.; Di Luccia, A. *Eur. J. Biochem.* 2002, 269, 4317−4325.
(4) Iacomino, G.; Picariello, G.; Sbrana, F.; Di Luccia, A.; Raiteri, R.; D'Agostino, L. *Biomacromolecules* 2011, 12, 1178−1186.
(5) D'Agostino, L. *Nanoscale* 2018, 10, 12268−12275.
(6) Kröger, N.; Deutzmann, R.; Bergsdorf, C.; Sumper, M. *Proc. Natl. Acad. Sci.* 2000, 97, 14133−14138.
(7) Kröger, N.; Lorenz, S.; Brunner, E.; Sumper, M. *Science* 2002, 298, 584−586.
(8) Herrera, S. E.; Agazzi, M. L.; Cortez, M. L.; Marmisollé, W. A.; von Bilderling, C.; Azzaroni, O. *Macromol. Chem. Phys.* 2019, 220, 1−10.
(9) Muzzio, N. E.; Pasquale, M. A.; Marmisollé, W. A.; Von Bilderling, C.; Cortez, M. L.; Pietrasanta, L. I.; Azzaroni, O. *Biomater. Sci.* 2018, 6, 2230−2247.
(10) Agazzi, M. L.; Herrera, S. E.; Cortez, M. L.; Marmisollé, W. A.; Azzaroni, O. *Colloids Surf., B* 2020, 190, 110895.
(11) Andreozzi, P.; Diamanti, E.; Py-Daniel, K. R.; Cáceres-Vélez, P. R.; Martinelli, C.; Politakos, N.; Escobar, A.; Muzi-Falconi, M.; Azevedo, R.; Moya, S. E. *ACS Appl. Mater. Interfaces* 2017, 9, 38242−38254.
(12) Huang, Y.; Lawrence, P. G.; Lapitsky, Y. *Langmuir* 2014, 30, 7771−7777.
(13) Diagboya, P. N.; Olu-Owolabi, B. I.; Zhou, D.; Han, B. H. *Carbon* 2014, 79, 174−182.
(14) Laucirica, G.; Marmisollé, W. A.; Azzaroni, O. *Phys. Chem. Chem. Phys.* 2017, 19, 8612−8620.
(15) Dressick, W. J.; Wahl, K. J.; Bassim, N. D.; Stroud, R. M.; Petrovykh, D. Y. *Langmuir* 2012, 28, 15831−15843.
(16) Irigoyen, J.; Moya, S. E.; Iturri, J. J.; Llarena, I.; Azzaroni, O.; Donath, E. *Langmuir* 2009, 25, 3374−3380.
(17) Pérez-Mitta, G.; Marmisollé, W. A.; Albesa, A. G.; Toimil-Molares, M. E.; Trautmann, C.; Azzaroni, O. *Small* 2018, 14, 1−8.
(18) Laucirica, G.; Pérez-Mitta, G.; Toimil-Molares, M. E.; Trautmann, C.; Marmisollé, W. A.; Azzaroni, O.; Phys, J. *Chem. C* 2019, 123, 28997−29007.
(19) Capdevila, D. A.; Marmisollé, W. A.; Tomasina, F.; Demicheli, V.; Portela, M.; Radi, R.; Murgida, D. H. *Chem. Sci.* 2015, 6, 705−713.
(20) Capdevila, D. A.; Marmisollé, W. A.; Williams, F. J.; Murgida, D. H. *Phys. Chem. Chem. Phys.* 2013, 15, 5386−5394.
(21) Béraud, A.; Sauvage, M.; Bazán, C. M.; Tie, M.; Bencherif, A.; Bouilly, D. *Analyst* 2021, 146, 403−428.
(22) Fenoy, G. E.; Marmisollé, W. A.; Azzaroni, O.; Knoll, W. *Biosens. Bioelectron.* 2020, 148, 111796.
(23) Zhang, X.; Jing, Q.; Ao, S.; Schneider, G. F.; Kireev, D.; Zhang, Z.; Fu, W. *Small* 2020, 16, 1−24.
(24) Piccinini, E.; Fenoy, G. E.; Cantillo, A. L.; Allegretto, J. A.; Scotto, J.; Piccinini, J. M.; Marmisollé, W. A.; Azzaroni, O. *Adv. Mater. Interfaces* 2022, 2102526, 2102526.
(25) Zhan, B.; Li, C.; Yang, J.; Jenkins, G.; Huang, W.; Dong, X. *Small* 2014, 10, 4042−4065.
(26) Fu, W.; Jiang, L.; van Geest, E. P.; Lima, L. M. C.; Schneider, G. F. *Adv. Mater.* 2017, 29, 1603610.
(27) Wu, G.; Dai, Z.; Tang, X.; Lin, Z.; Lo, P. K.; Meyyappan, M.; Lai, K. W. C. *Adv. Healthcare Mater.* 2017, 6, 1700736.
(28) Piccinini, E.; Bliem, C.; Reiner-Rozman, C.; Battaglini, F.; Azzaroni, O.; Knoll, W. *Biosens. Bioelectron.* 2017, 92, 661−667.

(29) Kwak, Y. H.; Choi, D. S.; Kim, Y. N.; Kim, H.; Yoon, D. H.; Ahn, S. S.; Yang, J. W.; Yang, W. S.; Seo, S. *Biosens. Bioelectron.* **2012**, *37*, 82−87.

(30) Fenoy, G. E.; Bilderling, C.; Knoll, W.; Azzaroni, O.; Marmisollé, W. A. *Adv. Electron. Mater.* **2021**, *7*, 2100059.

(31) Ramakrishna, T. R. B.; Nalder, T. D.; Yang, W.; Marshall, S. N.; Barrow, C. J.; Mater, J. *Chem. B* **2018**, *6*, 3200−3218.

(32) Sassolas, A.; Blum, L. J.; Leca-Bouvier, B. D. *Biotechnol. Adv.* **2012**, *30*, 489−511.

(33) Vakurov, A.; Simpson, C. E.; Daly, C. L.; Gibson, T. D.; Millner, P. A. *Biosens. Bioelectron.* **2005**, *20*, 2324−2329.

(34) Sheldon, R. A.; van Pelt, S. *Chem. Soc. Rev.* **2013**, *42*, 6223−6235.

(35) Chen, C.; Xie, Q.; Yang, D.; Xiao, H.; Fu, Y.; Tan, Y.; Yao, S. *RSC Adv.* **2013**, *3*, 4473−4491.

(36) Niyogi, S.; Bekyarova, E.; Itkis, M. E.; Zhang, H.; Shepperd, K.; Hicks, J.; Sprinkle, M.; Berger, C.; Lau, C. N.; Deheer, W. A.; Conrad, E. H.; Haddon, R. C. *Nano Lett.* **2010**, *10*, 4061−4066.

(37) Jesionowski, T.; Zdarta, J.; Krajewska, B. *Adsorption* **2014**, *20*, 801−821.

(38) Fenoy, G. E.; Marmisollé, W. A.; Knoll, W.; Azzaroni, O. *Sensors & Diagnostics* **2022**, *1*, 139−148.

(39) Berninger, T.; Bliem, C.; Piccinini, E.; Azzaroni, O.; Knoll, W. *Biosens. Bioelectron.* **2018**, *115*, 104−110.

(40) Tanaka, T.; Sakai, R.; Kobayashi, R.; Hatakeyama, K.; Matsunaga, T. *Langmuir* **2009**, *25*, 2956−2961.

(41) Mao, S.; Pu, H.; Chang, J.; Sui, X.; Zhou, G.; Ren, R.; Chen, Y.; Chen, J. *Environ. Sci. Nano* **2017**, *4*, 856−863.

(42) Yu, C.; Chang, X.; Liu, J.; Ding, L.; Peng, J.; Fang, Y. *ACS Appl. Mater. Interfaces* **2015**, *7*, 10718−10726.

(43) WO2021/240440, 2021.

(44) Maza, E.; Tuninetti, J. S.; Politakos, N.; Knoll, W.; Moya, S.; Azzaroni, O. *Phys. Chem. Chem. Phys.* **2015**, *17*, 29935−29948.

(45) Shen, Y.; Zhou, P.; Sun, Q. Q.; Wan, L.; Li, J.; Chen, L. Y.; Zhang, D. W.; Wang, X. B. *Appl. Phys. Lett.* **2011**, *99*, 2011−2014.

(46) Halthur, T. J.; Elofsson, U. M. *Langmuir* **2004**, *20*, 1739−1745.

(47) Fenoy, G. E.; Maza, E.; Zelaya, E.; Marmisollé, W. A.; Azzaroni, O. *Appl. Surf. Sci.* **2017**, *416*, 24−32.

(48) Piccinini, E.; Allegretto, J. A.; Scotto, J.; Cantillo, A. L.; Fenoy, G. E.; Marmisollé, W. A.; Azzaroni, O. *ACS Appl. Mater. Interfaces* **2021**, *13*, 43696−43707.

(49) Vörös, J. *Biophys. J.* **2004**, *87*, 553−561.

(50) Wang, Y. Y.; Burke, P. J. *Nano Res.* **2014**, *7*, 1650−1658.

(51) *Cold Spring Harb. Protoc.*, 2006, 2006, pdb.rec8247.

(52) Lawrence, P. G.; Lapitsky, Y. *Langmuir* **2015**, *31*, 1564−1574.

(53) Xu, S.; Zhang, C.; Jiang, S.; Hu, G.; Li, X.; Zou, Y.; Liu, H.; Li, J.; Li, Z.; Wang, X.; Li, M.; Wang, J. *Sens. Actuators, B* **2019**, *284*, 125−133.

(54) Sumner, J. B.; Hand, D. B. *J. Am. Chem. Soc.* **1929**, *51*, 1255−1260.

(55) Dervisevic, M.; Dervisevic, E.; Şenel, M. *Sens. Actuators, B* **2018**, *254*, 93−101.

(56) Buron, C. C.; Quinart, M.; Vrlinic, T.; Yunus, S.; Glinel, K.; Jonas, A. M.; Lakard, B. *Electrochim. Acta* **2014**, *148*, 53−61.

(57) Ono, T.; Kanai, Y.; Inoue, K.; Watanabe, Y.; Nakakita, S. I.; Kawahara, T.; Suzuki, Y.; Matsumoto, K. *Nano Lett.* **2019**, *19*, 4004−4009.

(58) Salvo, P.; Melai, B.; Calisi, N.; Paoletti, C.; Bellagambi, F.; Kirchhain, A.; Trivella, M. G.; Fuoco, R.; Di Francesco, F. *Sens. Actuators, B* **2018**, *256*, 976−991.

▣ Recommended by ACS